SHAKE-TABLE TEST OF A STRENGTHENED STONE MASONRY BUILDING AGGREGATE WITH FLEXIBLE DIAPHRAGMS.

Gabriele Guerrini
University of Pavia
Via Ferrata 3, Pavia, Italy
+39 0382 5169823
gabriele.guerrini@unipv.it

Ilaria Senaldi
University of Pavia
Via Ferrata 3, Pavia, Italy
+39 0382 5169823
ilaria.senaldi@unipv.it

Francesco Graziotti
University of Pavia
Via Ferrata 3, Pavia, Italy
+39 0382 5169823
francesco.graziotti@unipv.it

Guido Magenes
University of Pavia and European Centre for Training and Research in Earthquake Engineering (EUCENTRE)
Via Ferrata 3, Pavia, Italy
+39 0382 985450
guido.magenes@unipv.it

Katrin Beyer
Ècole Politechnique de Lausanne,
Bâtiment CE 3316, Station 1, CH - 1015 Lausanne, Switzerland
+41 21 69 36234
katrin.beyer@epfl.ch

Andrea Penna
University of Pavia and European Centre for Training and Research in Earthquake Engineering (EUCENTRE)
Via Ferrata 3, Pavia, Italy
+39 0382 5169824
andrea.penna@unipv.it

ABSTRACT

A unidirectional shake-table test was performed on the half-scale prototype of a natural stone masonry building aggregate, to investigate the seismic performance of this type of historical construction and to assess the effectiveness of two retrofit solutions. The specimen represented a building aggregate with two adjacent three-storey units, connected along one side as if they were built at different times. Double-leaf stone masonry with undressed blocks and river pebbles was used for the walls. Timber floors constituted flexible diaphragms in their planes. Roofs with different timber truss configurations and heights covered the two units. Improved wall-to-diaphragm connections and tie rods were pre-installed, although initially not fastened, on the prototype. Both retrofit systems were activated after significant damage was reached testing the unstrengthened specimen. This paper describes the seismic behaviour of the prototype, focusing on the effects of the retrofit interventions on damage mechanism evolution, lateral displacement demand, hysteretic response, and dynamic properties degradation.

Keywords: flexible diaphragm; half-scale shake-table test; historical building aggregate; natural stone masonry; seismic retrofit; tie rod; unreinforced masonry (URM); wall-to-diaphragm connection.

1. INTRODUCTION

In 1356 an earthquake devastated the city of Basel, with estimated moment magnitude of 6.6 (Fäh et al. 2009) and macroseismic intensity up to 9 on the European EMS-98 scale (Grünthal 1998). Reconstruction following this event resulted in the buildings that currently form most of the historical city centre. Nowadays, the seismic risk of the city of Basel is considered one of the highest in Switzerland, due to the combination of three main factors: (i) the seismic hazard of the region, which is moderately high within the Swiss context, despite not the worst (SIA 261:2014; Wiemer et al. 2016); (ii) the relatively vulnerable local building stock, in part dating back to the post-1356 earthquake reconstruction and mostly built before 1970, when the first Swiss seismic regulations were introduced; and (iii) a larger concentration of population and economic activities within the city compared to other areas of the country.

Several experimental campaigns have been conducted on stone masonry buildings, with or without retrofit interventions, in other seismic-prone European countries (Tomaževič et al. 1991; Benedetti et al. 1998; Mazzon et al. 2010; Magenes et al. 2010, 2014; Senaldi et al. 2014; Vintzileou et al. 2015; Mouzakis et al. 2018), but data lack regarding Northern-European historical construction practices. Moreover, these studies investigate mostly the performance of individual buildings without considering the interaction between adjacent structures, which form aggregates in historical city centres. The sporadic literature on the response of building aggregates is mainly limited to numerical investigations, following either simplified or more detailed modelling approaches (Senaldi et al. 2010; Maio et al. 2015; Formisano et al. 2015; Formisano 2017), or to case studies from assessment or reconstruction projects following real-life earthquakes (Carocci 2012, da Porto et al. 2013).

Hence, the Construction Department of the Canton of Basel City and the Swiss Federal Office for the Environment promoted a comprehensive research program, jointly carried out by the University of Pavia, Italy, and the École Polytechnique Fédérale de Lausanne, Switzerland. The project aims at providing tools for assessing and reducing the seismic vulnerability of Basel's heritage building stock, and at identifying effective retrofit solutions where necessary. The experimental program was conducted at the University of Pavia and at the EUCENTRE laboratories (Pavia, Italy). It culminated with an incremental unidirectional shake-table test on a half-scale, unreinforced masonry building aggregate prototype (Senaldi et al. 2019), with typical features of Basel's heritage residential buildings. After testing the unstrengthened masonry prototype up to severe damage conditions, two retrofit systems were activated to increase the input intensity: wall-to-diaphragm connections (Modena et al. 2005; Valluzzi 2007; Moreira et al. 2014; Moreira et al. 2016) and tie rods (Calderini et al. 2015; Calderini et al. 2019; Celik et al.2009; Magenes et al., 2010; Podestà and Scandolo, 2019; Tomaževič et al. 1996). As part of the experimental program, material and component tests were also performed for characterization purposes (Guerrini et al. 2017). This paper focuses on the main results of the shake-table tests and discusses the effects of the retrofit strategies on the seismic response of the prototype building.

2. DESCRIPTION OF THE PROTOTYPE

2.1.Geometry and construction details

Geometry and construction details of the tested prototype simulated typical features of the heritage residential buildings of the historical centre of Basel, which were usually built adjacent to one another at different times. The resulting façades are continuous along the

streets, while transverse party walls are shared among two adjacent units. The prototype building aggregate consists of two three-storey structural units with different roof heights and a common intermediate transverse wall. The prototype was constructed at half-scale because of the limited dimensions of the uniaxial shake-table of the EUCENTRE laboratory in Pavia, Italy. The entire structure was built directly on composite steel-concrete foundations bolted to the shake-table. The foundation surface was roughened to guarantee friction and bond between concrete and mortar at the bottom of the masonry walls. Soil-structure interaction effects were intentionally excluded by building the prototype on a rigid foundation. The prototype measured 5.97 m in the direction of uniaxial shaking (North-South), and 5.58 m in the transverse direction (East-West), with roof-ridge heights of 6.64 m and 7.54 m above the foundation for the North and South units, respectively (Figure 1a to d). The West and the East façades were oriented parallel to the direction of shaking, while the North, South and intermediate walls were excited out of plane. A steel frame, fixed to the table but not to the specimen, provided a safety restraint against unexpected collapses and a nearly-rigid reference system to measure displacements relative to the base.

The prototype was constructed with double-leaf undressed stone masonry (stone size of 100÷400 mm) arranged in almost horizontal courses, although not perfectly regular, with through-stones only near openings and corners. A volumetric ratio of 10÷15% of river pebbles (diameter of about 50 mm) was incorporated in the masonry. The perimeter wall thickness decreased along the height of the building: 350 mm at the ground storey, 300 mm at the second one, and 250 mm over the third storey and the gables; it reduced to 150 mm below all windows. The intermediate wall had constant thickness equal to 300 mm. The

opening layout is shown on Figure 1. Plaster was applied to the entire East façade, across the vertical joint of the West wall, and to portions of the first-storey interior walls.

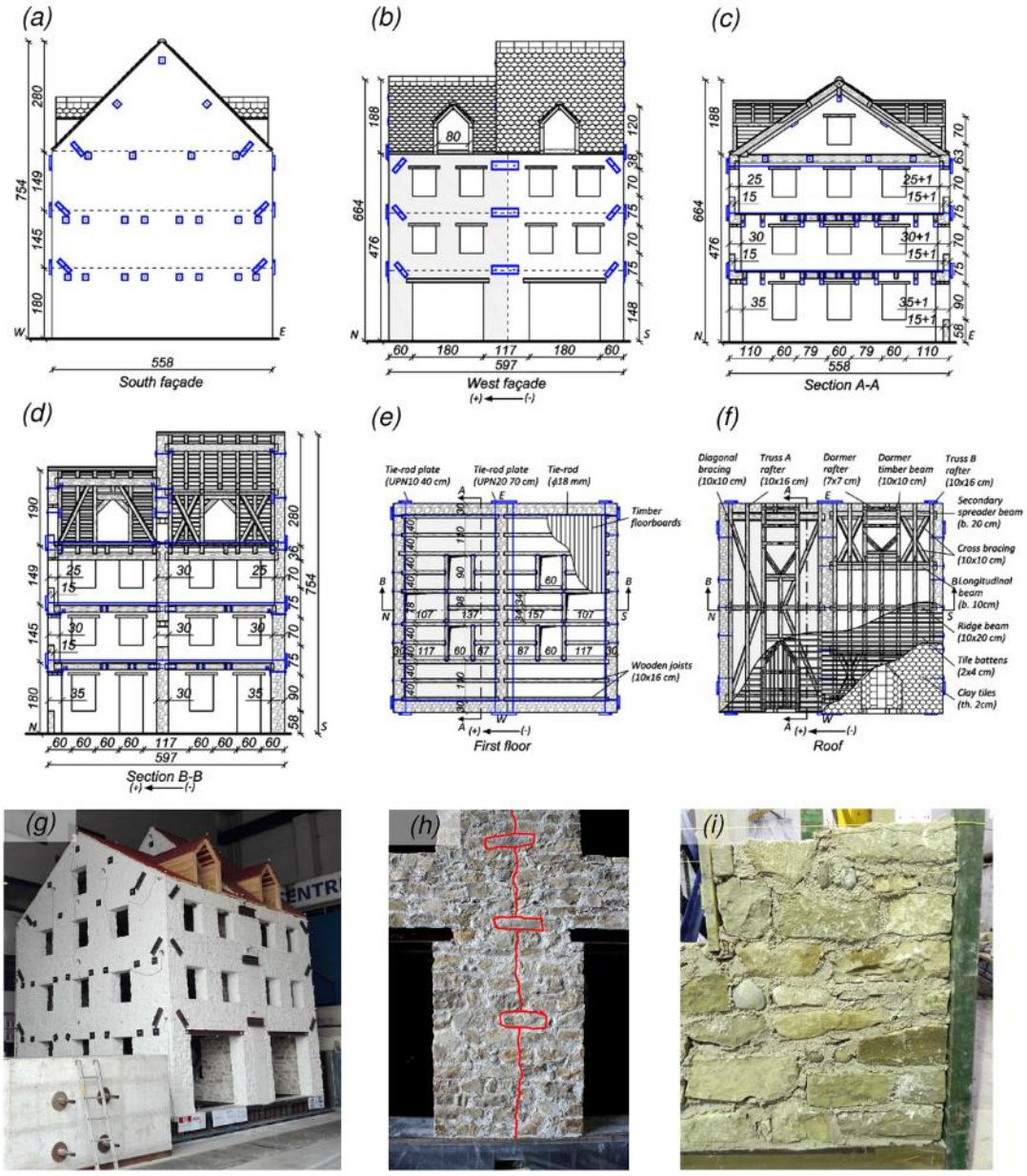

Figure 1. Building aggregate prototype: (a) South façade; (b) West façade; (c) section looking North; (d) section looking East; (e) first-floor plan; (f) roof plan; (g) photo of the North-West corner; (h) vertical joint between structural units on the West-wall outer leaf, marked in red. Units of cm.

Figure 2. Floor and roof diaphragms: (a) timber floor, view from below; (b) roof trusses with 45° slope; (c) clay tiles, tile battens, and dormers.

In order to simulate subsequent construction periods, the two structural units constituting the building aggregate were connected in correspondence of the shared transverse wall, at its intersection with the East and West façades (Figure 1b). Through-stones every third masonry course, alternatively located in the outer or inner masonry leaf, provided a weak vertical joint between the units (Figure 1f). The North building was assumed to be constructed first, and the South one later adjacent to it.

The first- and second-floor timber diaphragms consisted of 100 x 160 mm timber joists spanning in the North-South direction (parallel to shaking, see Figure 1e) and resting on the transverse walls, spaced at approximately 0.5 m. 20-mm-thick timber planks were nailed to the joists with two nails (2-mm diameter, 60-mm long) for each timber plank (Figure 2a). Floor openings allowed access and room for the steel frame inside the building. Timber trusses, oriented perpendicularly to the direction of shaking and resting on the West and East façades, constituted the main roof framing (Figure 1f). 100 x 200 mm timber spreader beams, embedded into the masonry thickness, transferred the truss reactions to the longitudinal walls. The truss tie beams served also as third-floor joists, to which the timber planks were nailed. Different truss configurations characterized the North and South roofs, with slopes of 34° and 45°, respectively. The trusses of the North roof had a simple triangular geometry, while the South trusses were more complex, with a collar tie beam

and a secondary structure constituted by secondary rafters and horizontal beams (Figure 2b). As typical for Basel historical buildings, the in-plane stiffness of the roof pitches was increased by inverted-V (North unit) or cross (South unit) bracings. Clay tiles were mounted on tile battens directly nailed to the truss rafters, without timber planks (Figure 2c). Four dormers completed the roof. Additional construction details can be found in Senaldi et al. (2019).

2.2.Retrofit solutions

Two strengthening solutions were chosen to improve the global seismic response of the building aggregate. A key selection criterion was to limit the intervention invasiveness, thus preserving the appearance and texture of heritage buildings. The structural objectives of the retrofit interventions were: (i) enhancing locally the connection between masonry walls or gables with floor or roof diaphragms; (ii) preventing partial or total collapses due to out-of-plane overturning mechanisms; (iii) coupling the response of the two units, hence promoting an overall box-type response of the entire building aggregate. The prototype building was first tested in the unstrengthened configuration up to a near collapse condition, as described in detail in Senaldi et al. (2019); then, the selected strengthening strategies were activated in subsequent phases.

The first retrofit strategy was an improvement of the wall-to-diaphragm connections (Modena et al. 2005; Valluzzi 2007; Moreira et al. 2014; Moreira et al. 2016), otherwise limited to the frictional resistance of joist supports. At the first two floors, the floor joists resting on masonry piers were connected to the North and South transverse walls with metallic elements (Figure 3a). 100-mm-wide steel angles (150 x 150 x 12 mm) were screwed to the joists and connected to an exterior steel anchor plate (140 x 150 x 10 mm)

by a M16 threaded rod, inserted in sleeves inside the masonry. Anti-shrinkage mortar allowed a uniform stress distribution between the steel angles and the interior side of the walls; for the same purpose, 16-mm-thick neoprene layers were located between the exterior anchor plates and the stone masonry.

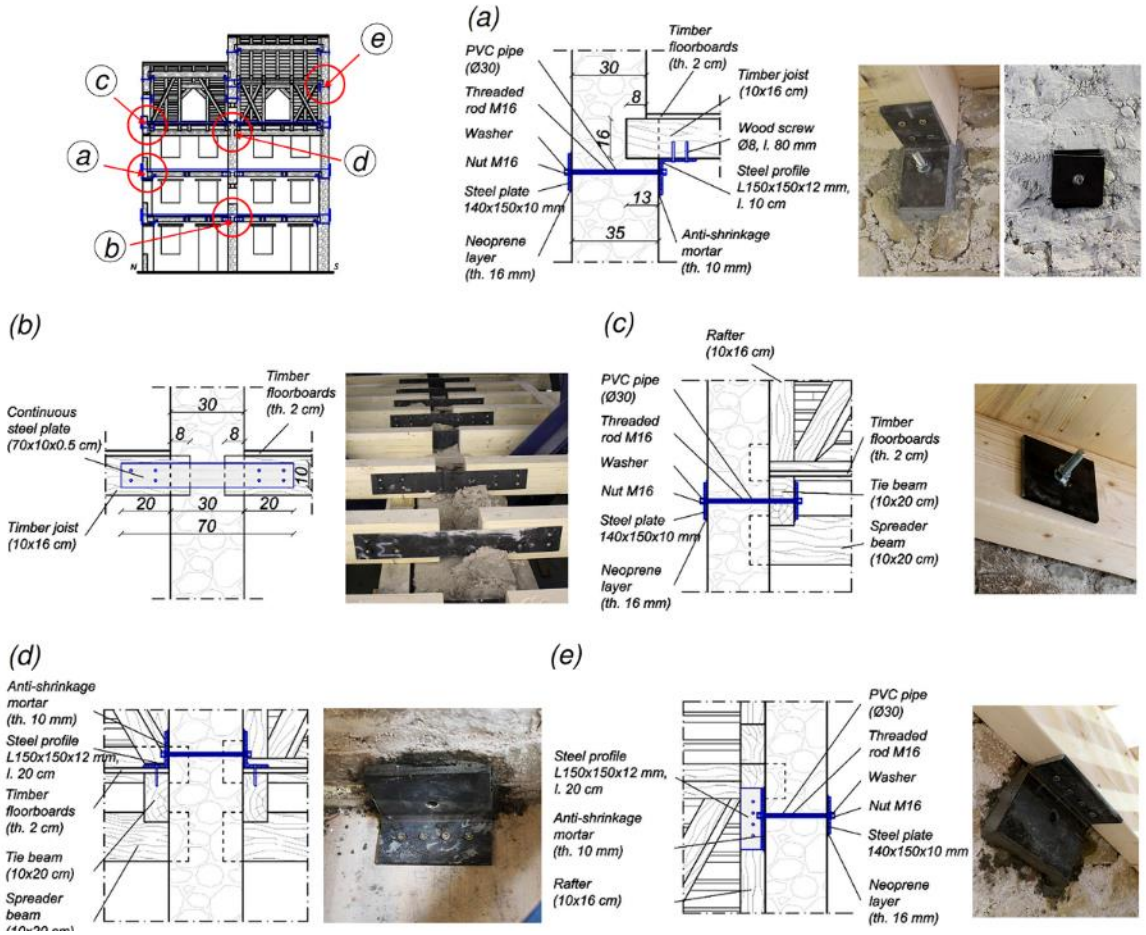

Figure 3. Wall-to-diaphragm connections (vertical sections and photos): (a) North and South walls to first- and second-floor joists or ridge beam; (b) transverse party wall to first- and second-floor joists; (c) North and South walls to roof-truss tie beam; (d) transverse party wall to roof-truss tie beam; (e) gables to roof-truss rafter. Units of cm, unless otherwise noted.

199 Rectangular steel plates (700 x 100 x 5 mm), screwed to the matching ends of floor joists,
200 provided connection between the North and South diaphragms through the party wall at
201 the first and second floors, as shown in Figure 3b. These plates have the same function as
202 the steel angles, enhancing the diaphragm-to-wall connection. However, they were
203 installed during construction of the prototype for safety reasons, to avoid accessing the
204 damaged building to fasten the retrofit. In fact, the rectangular plates provide active
205 connection only when the steel angles at the other extremities of the floor joists are tighten
206 to the external anchor plates. Since initially the threaded rods were only inserted in the
207 sleeves through the walls, without anchor plates and without fastening them, their effect
208 on the unstrengthened prototype behaviour was deemed negligible. This allowed testing
209 the building first in un-retrofitted conditions, as the diaphragm connections were
210 ineffective; subsequent fastening of the threaded rods allowed continuation of the testing
211 in strengthened configuration.
212 The connection between gable walls and adjacent trusses were similarly improved. Internal
213 steel angles and external rectangular anchor plates connected the ridge beams to the gables
214 as described for floor joists. The truss tie beams adjacent the North and South gables were
215 connected to the masonry by interior and exterior rectangular steel plates
216 (140 x 150 x 10 mm) at four different points about 1 m apart, as depicted in Figure 3c. The
217 truss tie beams next to the party wall and the rafters adjacent to the gable walls were
218 connected to the masonry similarly to the floor joists and ridge beams. In this case, 200-
219 mm-wide steel angles (150 x 150 x 12 mm) were screwed to the timber on the interior side,
220 and tied to an exterior anchor plate (140 x 150 x 10 mm) by a M16 threaded rod sleeved
221 inside the masonry (Figure 3d and e). As for the lower storeys, the threaded rods were

initially inserted without fastening them against the exterior anchor plates, to allow testing the prototype in unretrofitted conditions.

The second strengthening system consisted of metallic tie rods located at each floor level, as shown in Figure 4, obtained from Dywidag 18WR post-tensioning threaded bars. This technique, traditionally applied to absorb arch thrusts, has proved effective in increasing the lateral displacement capacity (Calderini et al. 2015; Calderini et al. 2019). Also these rods were pre-installed within 30-mm-diameter ducts through the masonry thickness during construction, but initially left without anchor plates. They were manually post-tensioned only after testing with active wall-to-diaphragm connections, to allow increasing further the intensity of shaking.

To ensure good transmission of stresses between rods and masonry, UPN steel profiles were used as anchor plates, with the flanges serving as stiffeners. In particular, 400-mm-long UPN80 were used for the tie rods running along the perimeter walls (Figure 4a and b), while 660-mm-long UPN200 connected the rods running adjacent to the transverse party wall (Figure 4c) across the joint. The transverse tie rods of the South unit were located 150 mm away from the party wall, to avoid additional discontinuities in correspondence of the vertical joint and to induce less stress concentration at the edges of this unit's longitudinal walls, which were not built integrally with the party one. The tie rods ran parallel to the masonry walls in the longitudinal and transverse directions above the floor planks (Figure 1e), except for the third-floor transverse rods which were mounted below the diaphragm. Conflicts between orthogonal rods were eliminated by placing the ducts in the masonry at slightly different heights above the floor surface (Figure 4d).

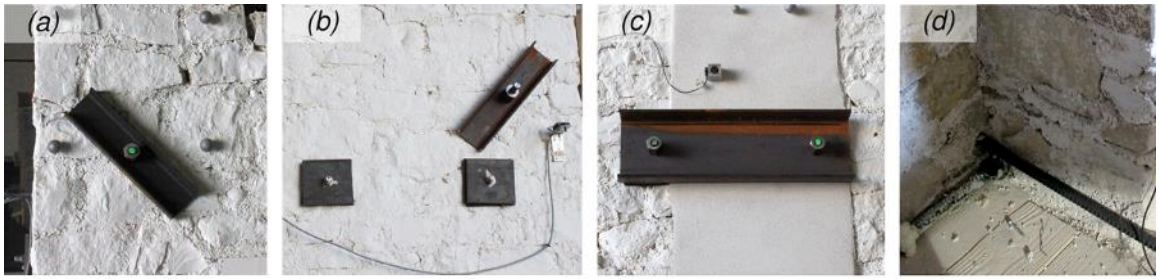

Figure 4. Tie rods: (a) steel anchor of a single tie rod, West façade; (b)) steel anchor for a single tie rod and anchor plates for diaphragm connections, North façade; (c) steel anchor for two tie rods adjacent to the vertical structural joint, West façade; (d) perpendicular tie rods crossing above the timber floor.

2.3.Similitude requirements and material properties

Conducting dynamic tests on reduced-scale specimens required the adoption of appropriate scaling factors. Due to laboratory constraints, a geometric length scale factor $\lambda = 0.5$ was selected. It was also decided to keep accelerations and mass densities unaltered, to avoid issues with gravity force scaling and shake-table payload (Senaldi et al. 2019). Therefore, time needed to be scaled by a factor $\lambda^{1/2} = 0.707$, while stress by the same factor $\lambda = 0.5$ adopted for lengths.

Because of the selected scaling factors, masonry strengths and elastic moduli needed to be reduced by $\lambda = 0.5$, with respect to the reference mechanical properties. This task was accomplished by selecting a suitable mortar composition, consisting of a pre-mixed natural hydraulic lime mortar with the addition of expanded polystyrene (EPS) beads in a ratio of 40% by volume. Credaro-Berrettino sedimentary stones from the area of Bergamo, Italy, and river pebbles completed the masonry.

A series of masonry characterization tests (Guerrini et al. 2017; Senaldi et al. 2019) resulted in mean compressive strength $f = 1.30$ MPa, tensile strength $f_t = 0.17$ MPa, Young's modulus $E = 3462$ MPa, Poisson's ratio $\upsilon = 0.14$, and shear modulus $G = 1898$ MPa (from diagonal compression tests) or $G = 1524$ MPa (from vertical compression tests).

Steel lintels were made of S275JR steel. M16 threaded rods for the wall-to-diaphragm connections were class 4.6, while plates and angles were made of S235JR and S355JR steel, respectively; timber screws had shear strength of 3.84 kN. The Dywidag 18WR tie rods were made of Y1050 steel and their anchorages were obtained from S235JR steel UPN profiles.

2.4.Masses

The total mass of the prototype was 82.0 t (Senaldi et al. 2019). More specifically, masonry had mean density of 1980 kg/m^3, so the walls provided a 72.0-t mass. Timber floors and finished roofs resulted in masses of 1.75 t and 3.75 t, respectively. A uniformly distributed mass of 1.5 t, representing non-structural dead loads and a portion of live loads, was added over each floor: mortar bags were used for this scope, to avoid increasing the diaphragm stiffness.

3. SHAKE-TABLE TESTS

3.1.Instrumentation

A dense number of sensors recorded the dynamic response of the specimen. 41 accelerometers monitored the in-plane and out-of-plane accelerations of the masonry walls. 72 linear and 16 wire potentiometers recorded floor and roof displacements, transverse walls out-of-plane displacements, sliding between joists and walls, and in-plane deformations of selected piers and spandrels. A load cell monitored the tensile force on one of the tie rods parallel to the shaking direction.

A three-dimensional optical motion-capture system (Vicon Motion Systems 2016) allowed determination of global displacements and local deformations of the building prototype. 16

fixed cameras recorded the 3D trajectories of 179 passive spherical markers coated with a retro-reflective material, located on the West, North, and South façades.

3.2.Testing protocol

The shake-table applied a series of ground motion records with increasing intensity to the base of the prototype. Three different natural accelerograms were chosen and progressively scaled in acceleration amplitude to the desired PGA (Senaldi et al. 2019). Main-shock test were alternated with random noise and calibration tests. These allowed identifying the dynamic properties of the structure under evolving damage conditions as well as tuning the shake-table control system.

The first two natural signals were recorded during recent low-intensity seismic events in Switzerland. The one identified as "BAS" (PGA of 0.072 g) was the E-W component recorded at the SBAJ station in Basel during a M_L 3.4 earthquake in December 2006 (Ripperger et al., 2009). The record labelled "LIN" (PGA of 0.087 g,) was the N-S component of the M_w 4.7 seismic event occurred in the Linthal valley in March 2017, recorded at the CH.SLTM2 station in Linthal (SED Strong motion portal, 2017). The third signal, named "MON" (PGA of 0.224 g) was the E-W component recorded at the Ulcinj-Hotel Albatros station during the 1979, M_w 6.9 Montenegro earthquake; this record was characterized by good compatibility with the elastic design displacement spectrum (Figure 5) associated with a return period of 475 years for the Basel Holocene sub-zone of the city of Basel (Fäh 2006; Fäh and Wenk 2009; Wenk and Fäh 2012). Similitude laws required compressing the digitization time step for all natural signals by a factor of $\lambda^{1/2} = 0.707$, being $\lambda = 0.5$ the scale factor applied to geometric lengths.

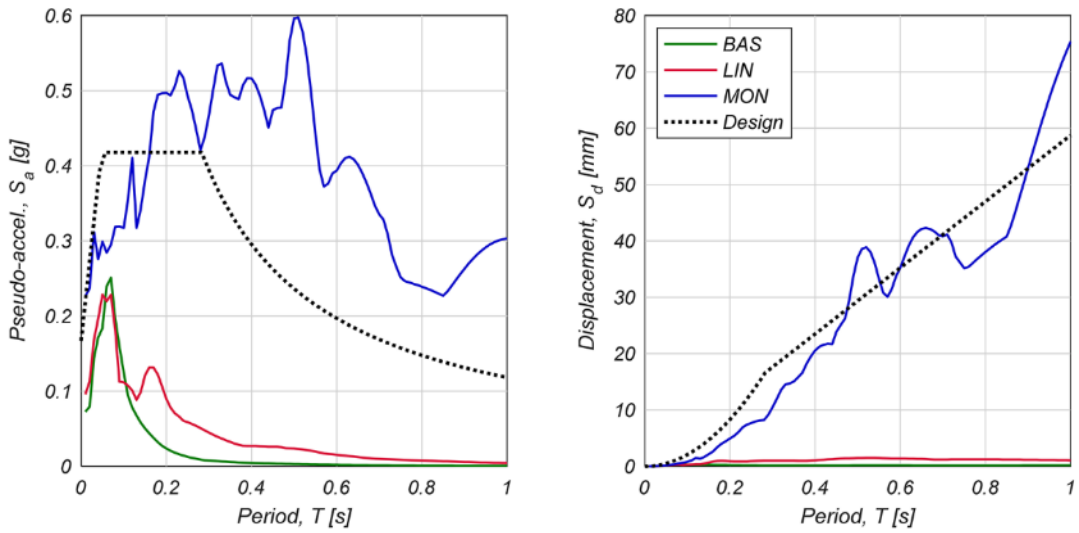

Figure 5. Elastic response spectra for 5% viscous damping ratio of the selected input signals and comparison with the 475-years return period design spectrum for Basel. Periods are scaled to comply with similitude relationships.

Table 1 summarizes the incremental sequence of main shocks imposed on the building specimen. The actual pseudo-spectral acceleration for 5% damping ratio, S_a, is referred to the fundamental period obtained in undamaged conditions ($T_{1,und}$ = 0.18 s) and in damaged conditions, ($T_{1,i}$), evaluated at the end of each i^{th} test through modal identification procedures. The longest fundamental period was measured at the end of test #42, before activation of the retrofit interventions ($T_{1,42}$ = 0.53 s). The average pseudo-spectral acceleration, $S_{a,avg}$, between $T_{1,und}$ and $T_{1,42}$ is defined as the geometric mean of the pseudo-acceleration spectrum according to Bianchini et al. (2009). The cumulative absolute velocity, CAV, and the Arias intensity, I_A (Arias 1970), are also reported in Table 1.

Table 1. Shake-table main testing sequence with intensity measures.

Test #	Test ID	Nominal PGA [g]	Recorded PGA [g]	CAV [m/s]	PGV [m/s]	$S_a(T_{1,und})$ [m/s^2]	$S_a(T_{1,i})$ [m/s^2]	$S_{a,avg}$ [m/s^2]	I_A [m/s]	*mHI* [mm]
10	BAS-100%	0.07	0.06	0.24	0.01	0.03	0.03	0.01	0.01	2.60
16	LIN-100%	0.09	0.05	0.23	0.01	0.12	0.06	0.04	0.01	6.09
19	MON-25%	0.06	0.05	1.14	0.04	0.11	0.11	0.11	0.03	9.71
21	MON-50%	0.11	0.10	2.60	0.08	0.28	0.20	0.24	0.13	20.9
26	MON-75%	0.17	0.17	4.60	0.14	0.47	0.31	0.40	0.39	34.7
29	MON-100%	0.22	0.20	4.77	0.16	0.44	0.38	0.43	0.43	36.4
33	MON-125%	0.28	0.27	6.36	0.21	0.58	0.62	0.61	0.76	53.6
37	MON-150%	0.34	0.32	7.43	0.24	0.58	0.66	0.66	1.00	58.0
42	MON-175%	0.39	0.35	8.73	0.29	0.81	0.87	0.81	1.39	66.2
47	MON-175%DC	0.39	0.34	8.56	0.29	0.82	0.91	0.82	1.36	67.1
53	MON-175%TR1	0.39	0.35	8.77	0.29	0.80	0.90	0.81	1.41	66.5
59	MON-175%TR2	0.39	0.37	9.03	0.30	0.81	0.82	0.84	1.49	68.7
64	MON-225%	0.50	0.51	11.48	0.37	1.06	1.22	1.07	2.36	85.9
74	MON-275%	0.61	0.64	13.90	0.45	1.28	1.60	1.34	3.59	107

Because of the good correlation with the nonlinear displacement demand on short-period unreinforced masonry structures (Graziotti et al. 2016), a modified Housner intensity, *mHI* (Magenes et al. 2014), was calculated as the integral of the pseudo-velocity spectrum at 5% viscous damping between 0.07 s and 0.35 s. This range is consistent with the fundamental periods typical of masonry structures, accounting for the time scaling factor $\lambda^{1/2} = 0.707$. The significant duration (Bradley 2011; Hancock et al. 2006) of the input signals was evaluated as the time interval between the development of 5% and 75% of I_A and between 5% and 95% of I_A, respectively named as $D_{5\text{-}75}$ and $D_{5\text{-}95}$. When scaled in time to account for similitude laws, the Montenegro input had nominal $D_{5\text{-}75}$ = 5.44 s and $D_{5\text{-}95}$ = 8.66 s. More details about the intensity measures can be found in Senaldi et al. (2019).

Test MON-175% was first conducted on the unstrengthened masonry structure. The same input signal was then applied after activation of the wall-to-diaphragm connections (test

MON-175%DC), and after tensioning the tie rods to two different force levels: 7.6 kN for MON-175%TR1 and 29 kN for MON-175%TR2. Tests MON-225% and MON-275% were performed with diaphragm connections activated and tie rods tensioned to 25 kN and 26 kN, respectively. These tie prestressing force values were measured by a load cell, installed in series with one of the longitudinal rods, at the beginning of each test, after any time-dependent losses occurred between tensioning and testing.

4. TEST RESULTS

4.1.Structural damage evolution

Details about damage experienced by the unstrengthened masonry structure can be found in Senaldi et al. (2019). The prototype first suffered minor structural damage during test MON-100% (PGA of 0.20 g), evidenced by hairline diagonal and vertical cracks in most spandrels of the West façade and in some spandrels of the East wall. Hairline cracks were visible also at the base of the northernmost and central pier of the West façade, and around timber lintels, joist supports, and steel lintel supports.

Extensive structural damage was experienced during test MON-175% (PGA of 0.35 g), that affected the spandrels of the longitudinal East and West façades significantly (Figure 6), with residual crack widths of 3÷7 mm, de-cohesion of some blocks, and permanent horizontal elongations up to 15 mm at the second-floor spandrel level on the two units. Differential displacements between the two units resulted in cracks extending upwards from the top corners of the third-storey windows towards the structural joint; a residual separation up to 14.5 mm was recorded at the top of the structural joint on the West façade. The piers of the longitudinal walls exhibited flexural-rocking response, evidenced by nearly horizontal cracks at their top and bottom, with residual widths of approximately

0.1 mm at the base 2÷3 mm at upper storeys. The flexible floor diaphragms experienced significant in-plane deformation due to the differential displacement between the two longitudinal walls, induced by the different size and asymmetric distribution of openings and piers at the first storey.

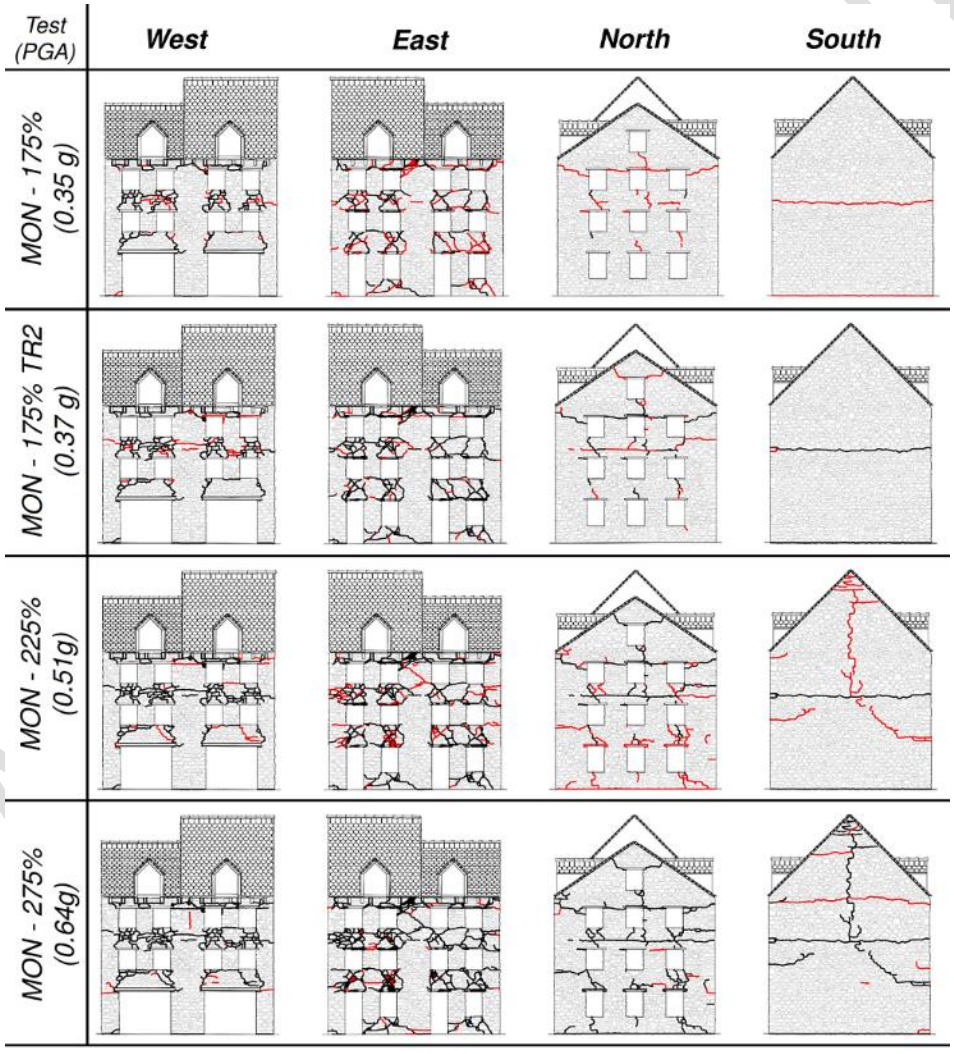

Figure 6. Evolution of the crack pattern. Crack segments marked in red opened during the current test. Crack segments marked in black had been previously detected.

Out-of-plane mechanisms first occurred during the test MON-175%, in the upper portions of both North and South façades. Horizontal cracks opened at the top of the North façade, due to the out-of-plane overturning of the gable, in correspondence of the third-story lintels and extended to the base of the gable wall. Some cracks were detected at the second-floor level of the North facade, anticipating a possible multiple-block rocking mechanism. Cracks formed also in all spandrels of the North wall. On the South façade, instead, the mechanism activated at the second-floor level, where the masonry thickness decreased from 300 mm to 250 mm and a 1-mm residual width was measured along a horizontal crack. Hairline horizontal cracks opened at the interface between the foundation and the South wall. Floor joists slid with respect to the transverse North and South walls, with a residual slip at the second floor level of about 4.8 mm and 9.1 mm, respectively. Due to interlock between intersecting walls, the southernmost piers of the East and West façades participated in the overturning mechanism of the South façade.

Because of the severe level of damage experienced by the specimen, the retrofit interventions previously installed were activated prior to reach near-collapse conditions, allowing continuation of the testing campaign. Fastening the wall-to diaphragm connections and post-tensioning the tie rods resulted in almost complete recovery of residual displacements, floor joist slip, and residual cracks. Hence, the test with Montenegro input scaled at 175% was repeated first after the activation of the wall-to-diaphragm connections and later after post-tensioning the tie rods at two different forces. After test MON-175%DC and test MON-175%TR1 the damage pattern remained substantially unvaried with respect to test MON-175%, except for minor elongation and widening of pre-existing cracks, which was nevertheless partially recovered with the post-

401 tensioning operations. The diaphragm connections allowed significant reduction of the
402 residual floor joists slip, which reduced from 9.1 mm to 0.5 mm after test MON-175%DC
403 and 0.2 mm after test MON-175%TR1, at the second floor level of the South wall.
404 After test MON-175%TR2, the level of damage in the spandrels increased, with further
405 elongation and widening of existing cracks and opening of new ones (Figure 6). Flexural-
406 rocking response of the central pier at third storey of the West façade was detected. New
407 cracks due to out-of-plane overturning mechanisms appeared also in the North façade: in
408 particular, they became more evident at the second-floor level, where the masonry
409 thickness decreased from 300 mm to 250 mm. An overturning mechanism involving the
410 upper portion of the North gable above the timber lintel was evidenced by inclined cracks
411 originating from the upper corners of the gable window.
412 Combining improved wall-to-diaphragm connections with post-tensioning of the tie rods
413 before each test, permitted to further increase the shaking intensity. Two-way out-of-plane
414 bending of the transverse North and South façades was evidenced by the crack pattern
415 detected after test MON-225% (PGA of 0.50 g), as shown in Figure 6. In the North façade,
416 horizontal cracks opened at the interface between the foundation and the masonry wall,
417 while nearly vertical and diagonal cracks in the spandrels increased in number and extent
418 due to the out-of-plane two-way bending deformation of the wall. A typical two-way out-
419 of-plane bending damage pattern was visible in the South façade, with a vertical crack in
420 the centre above the second floor level and with inclined and horizontal cracks at the second
421 storey. Nevertheless, because of the presence of the steel anchors and of the tie rods, the
422 maximum residual second-floor joist slip was limited between 0.1 and 0.15 mm in
423 correspondence of the North and South façades, respectively. Significant damage was also

recorded in the spandrels of the longitudinal façades, with residual crack width of 2÷5 mm. Diagonal cracks formed through the central third-storey pier of the East façade, crossing the vertical joint between the structural units and connecting windows corners, likely caused by third-storey relative displacements between the two portions of the aggregate. Diffuse hairline cracking was detected in the masonry close to the ridge beam support in the South gable. Portions of plaster detached and fell from the spandrels of the East façade during the test.

Near-collapse conditions were reached by the strengthened building prototype during test MON-275% (PGA of 0.64 g). Because of the in-plane and out-of-plane response of the prototype, diffuse cracking was visible in piers and spandrels (Figure 7d, f and h). A general elongation of pre-existing cracks was detected in the longitudinal walls, although the effectiveness of the tie rods limited the residual crack width to a maximum of 10 mm in the West wall and of 7 mm in the East façade. Spandrels and piers of the longitudinal façades were, nevertheless, significantly affected by a general de-cohesion of masonry, with fall of small stones, portions of mortar, and debris (Figure 7c, d and g). Further detachment of plaster in the East façade occurred during the test (Figure 7c and e). A vertical crack appeared in the central third-storey piers of the West wall because of the separation between the two structural units along the joint (Figure 7c and d).

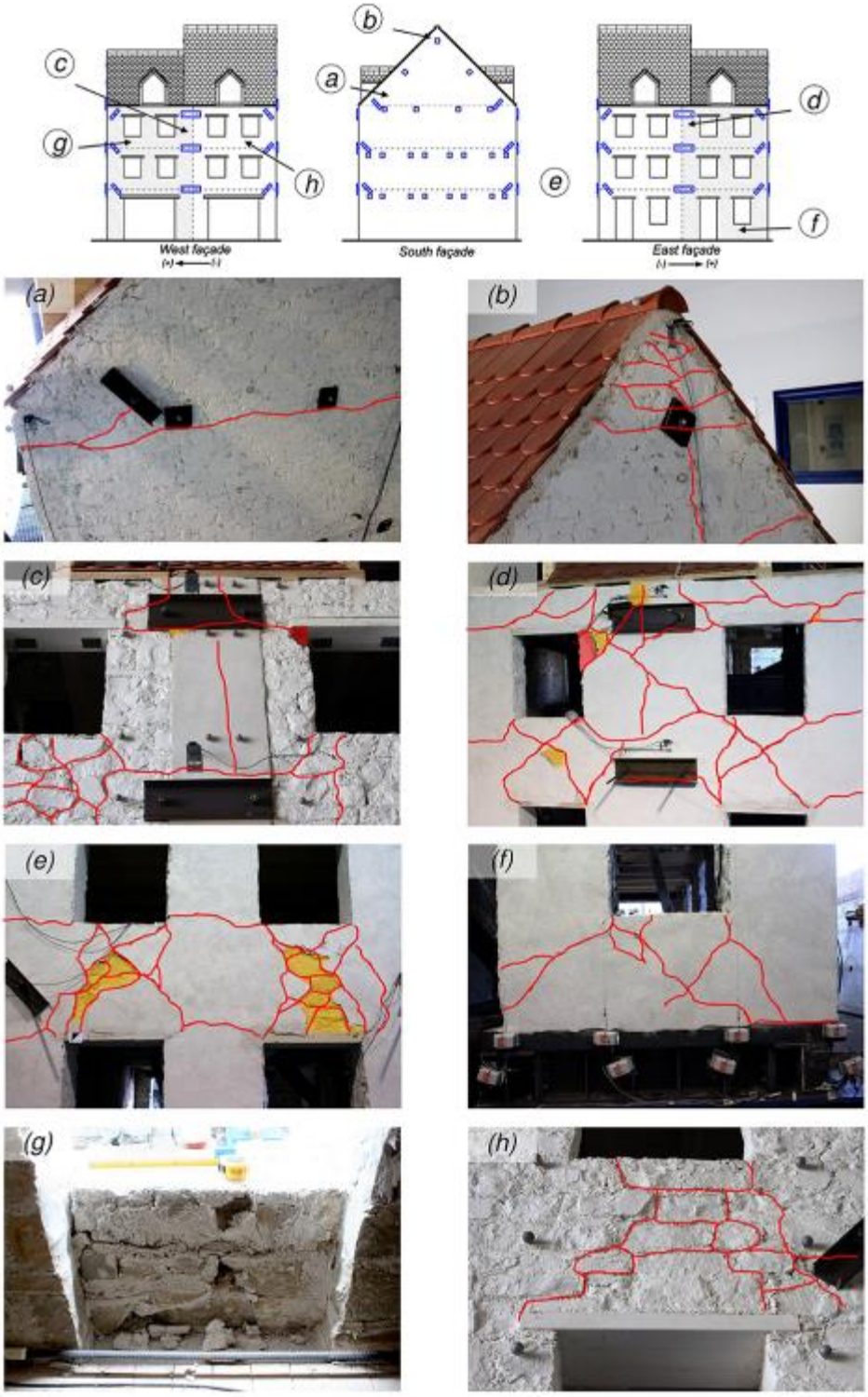

Figure 7. Observed damage pattern at the end of test MON-275%: (a), (b) out-of-plane overturning cracks on the South gable wall; (c), (d) crack pattern on the central pier of the West and East walls, respectively, with vertical cracks in correspondence of the structural joint; (e) damage in the East wall spandrels at the first-floor level; (f) flexural cracks at the base of the northern piers of the East façade; (g), (h) de-cohesion of stones in the West façade spandrels. Cracks marked in red opened or widened during the test; red-shaded areas represent detachment of stones, yellow-shaded areas detachment of plaster.

The out-of-plane response of the South wall determined the opening of new horizontal cracks in correspondence of the third floor (Figure 7a) and of the secondary tie beam of the southernmost roof truss. Widening of the residual cracks up to 2 mm was detected on the South gable in correspondence of the ridge beam (Figure 7b). Residual timber-lintel dislocations of 10÷30 mm were recorded above the gable opening and the central third-storey window of the North façade at the end of the test. The northernmost and southernmost second- and third-storey piers of the East and West façades participated as return walls with flange effect in the overturning mechanisms of the transverse façades. This response is evidenced by the damage pattern: the horizontal cracks that formed at the top and bottom of such piers at each storey joined the cracks that developed on the transverse façades in correspondence of the overturning portions. The retrofit interventions limited the residual slip of floor joists to approximately 0.2 mm at the first- and second-floor levels of both transverse façades. A 3.8-mm residual slip of the spreader beam embedded above the West masonry wall, supporting the South roof, was recorded.

4.2.In-plane response of longitudinal façades

The longitudinal-wall crack pattern denoted damage concentrating in the spandrels. The elongation of the West façade at the level of the second-floor spandrels was measured taking the difference between the displacements of the reflective markers located at the façade corners, and those of the markers adjacent to the vertical joint. Figure 8a and b presents the time-histories of the elongations recorded during the tests with the MON signal scaled at 175%, for the unstrengthened masonry building (MON-175%, PGA of 0.35 g) and after activation of the diaphragm connections (MON-175%DC, PGA of 0.34 g) and tie rods (MON-175%TR2, PGA of 0.37 g). For the sake of comparison, the elongation was

zeroed at the beginning of each test; in other words, residual deformations cumulated during previous tests were discarded. The figure confirms the effectiveness of both types of intervention in reducing residual elongations: in particular, on the South façade they reduced from 7.6 mm without any retrofit, to 1.4 mm with diaphragm connections and to about 0.2 mm with tie rods. During the final test (MON-275%, PGA of 0.64 g), the elongation of the South façade of the strengthened specimen reached a peak of 5.1 mm and a residual of 0.9 mm.

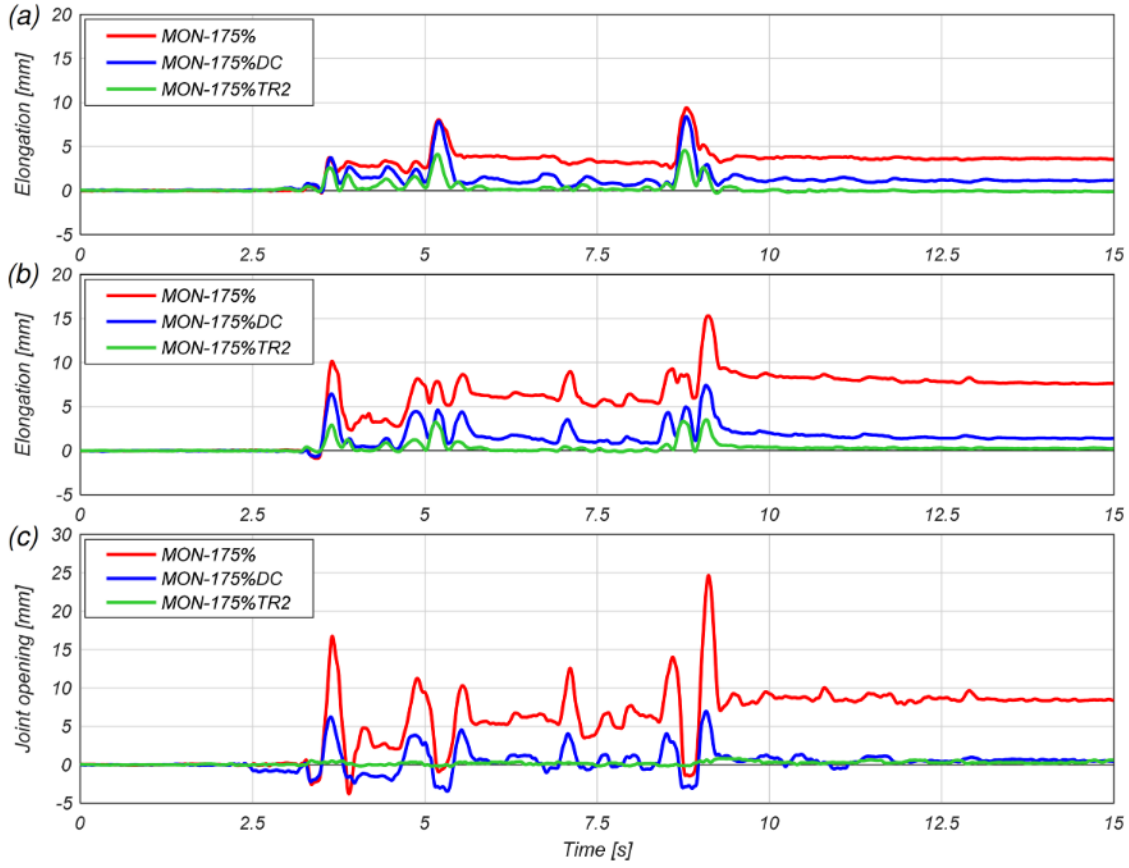

Figure 8. Time-history of West-façade response during tests with "MON" signal scaled at 175% before and after activation of the retrofit interventions: (a) elongation at the second-floor spandrel level in the North structural unit; (b) elongation at the second-floor spandrel level in the South structural unit; (c) crack opening across the structural joint at the third-floor level.

Interaction between the two structural units resulted in cracks at the top of the vertical joints of the longitudinal walls. The reflective markers adjacent to the joint on the West façade were used to measure the width of these cracks. Figure 8c shows the time-histories of the joint opening recorded during the tests with the MON signal scaled at 175% (PGA of about 0.35 g), before and after the activation of the retrofit interventions, discarding any cumulative residual crack width from previous tests. Both solutions proved effective in reducing the residual joint crack width to less than 1 mm at the end of the seismic excitation, while a residual opening of 8.5 mm was recorded on the unstrengthened structure. In the last test on the retrofitted prototype (MON-275%, PGA of 0.64 g), after reaching a peak of 1.5 mm, the joint did not present any residual opening.

4.3.Definition of engineering demand parameters

Lateral displacements recorded by the potentiometers were used to evaluate several engineering demand parameters listed in Table 2. In particular, $\delta_{i,E}$, $\delta_{i,W}$, $\delta_{i,N}$, and $\delta_{i,S}$ are the longitudinal displacements of the four perimeter walls at the i_{th} floor level with respect to the foundation (represented by the nearly-rigid steel frame), with $\delta_{i,N}$, and $\delta_{i,S}$ measured near mid-span of the transverse walls. Instead, $\delta_{R,N}$ and $\delta_{R,S}$ are the North and South roof-ridge displacements relative to the foundation, respectively. In order to obtain in-plane drift ratios or out-of-plane rotations, interstorey lateral displacements were normalized with respect to the corresponding interstorey height, h_i, or to the North and South roof-ridge heights above the third floor, $h_{R,N}$ and $h_{R,S}$. Roof in-plane shear deformations were obtained normalizing the ridge displacements relative to the third floor by the North and South roof rafter lengths, $l_{R,N}$ and $l_{R,S}$.

Table 2. Engineering demand parameters.

Definition	Equation
i^{th}-floor average displacement	$\delta_{i,AVG}=\frac{\delta_{i,E}+\delta_{i,W}}{2}$
i^{th}-storey drift ratio, East longitudinal wall	$\theta_{i,E}=\frac{\delta_{i,E}-\delta_{i-1,E}}{h_i}$
i^{th}-storey drift ratio, West longitudinal wall	$\theta_{i,W}=\frac{\delta_{i,W}-\delta_{i-1,W}}{h_i}$
i^{th}-storey average drift ratio	$\theta_{i,AVG}=\frac{\theta_{i,E}+\theta_{i,W}}{h_i}$
i^{th}-storey out-of-plane rotation, North transverse wall	$\theta_{i,N}=\frac{\delta_{i,N}-\delta_{i-1,N}}{h_i}$
i^{th}-storey out-of-plane rotation, South transverse wall	$\theta_{i,S}=\frac{\delta_{i,S}-\delta_{i-1,S}}{h_i}$
North gable out-of-plane rotation	$\theta_{R,N}=\frac{\delta_{R,N}-\delta_{3,AVG}}{h_{R,N}}$
South gable out-of-plane rotation	$\theta_{R,S}=\frac{\delta_{R,S}-\delta_{3,AVG}}{h_{R,S}}$
North roof-pitch in-plane shear deformation	$\gamma_{R,N}=\frac{\delta_{R,N}-\delta_{3,AVG}}{l_{R,N}}$
South roof-pitch in-plane shear deformation	$\gamma_{R,S}=\frac{\delta_{R,S}-\delta_{3,AVG}}{l_{R,S}}$
East longitudinal wall global drift ratio	$\tilde{\theta}_E=\frac{\delta_{3,E}}{\sum_{i=1}^{3} h_i}$
West longitudinal wall global drift ratio	$\tilde{\theta}_W=\frac{\delta_{3,W}}{\sum_{i=1}^{3} h_i}$
Average global drift ratio	$\tilde{\theta}_{AVG}=\frac{\tilde{\theta}_E+\tilde{\theta}_W}{2}$
Base shear	$V_B=\sum_j (a_i \cdot m_i)$
Base-shear coefficient	$BSC=\frac{V_B}{g \cdot m_i}=\frac{\sum_j (a_i \cdot m_i)}{g \cdot m_i}$

The strength of the prototype was expressed in terms of base shear and normalized base-shear coefficient, obtained from the products of the acceleration recorded by the j^{th} accelerometer, a_j, and the tributary mass associated with that instrument, m_j. The total mass $m_{TOT} = \sum m_j = 70.4$ t excludes the inertia of the lower half of the first storey walls, which were assumed to move solidly with the shake-table.

518 **4.4.Displacement response of the prototype**

519 Figure 9 shows the envelopes of interstorey drift ratios and floor displacements recorded
520 during the tests with the MON signal scaled at 175%, before and after the activation of the
521 retrofit interventions. Positive values correspond to the prototype leaning northward,
522 negative values leaning southward. All residual displacements cumulated by the un-
523 retrofitted structure during main-shock and calibration tests were accounted for up to test
524 MON-175%. It should be noted that activation of wall-to-diaphragm connections and tie
525 rods resulted in almost complete recover of residual deformations. For this reason, the
526 envelopes relative to tests in these configurations (MON-175%DC and MON-175%TR2)
527 were plotted neglecting any previous residual displacement.

528 During test MON-175% (PGA of 0.35 g) in the unstrengthened configuration, the
529 interstorey drift-ratio and floor displacement profiles of the four perimeter walls differed
530 from each other. The longitudinal West wall offered lower stiffness as expected from the
531 presence of wide ground-floor doors, with maximum drift ratios (between 1.0% and 1.5%)
532 that were approximately 1.5 times those experienced by the East wall (between 0.62% and
533 1.1%). Moreover, the positive and negative envelopes for the North and South walls were
534 significantly unsymmetrical, indicating separation between the opposite transverse walls
535 with the tendency to overturn outwards: for instance, the maximum third-floor
536 displacement in the positive (northward) direction was 65 mm for the North façade and 44
537 mm for the South one, with a separation of at least 21 mm; in the negative (southward)
538 direction, 54 mm were recorded on the South wall and 35 mm on the North one, with a
539 difference of 22 mm. The maximum out-of-plane rotations of the transverse walls at the
540 third storey (1.8% to 2.2%) were similar to those of the gables (1.9% to 2.2%) and about
541 twice those measured at the first two storeys (0.87% to 1.1%): this confirmed participation

of the third-storey transverse walls in the gable overturning mechanism, hinging at the second-floor level.

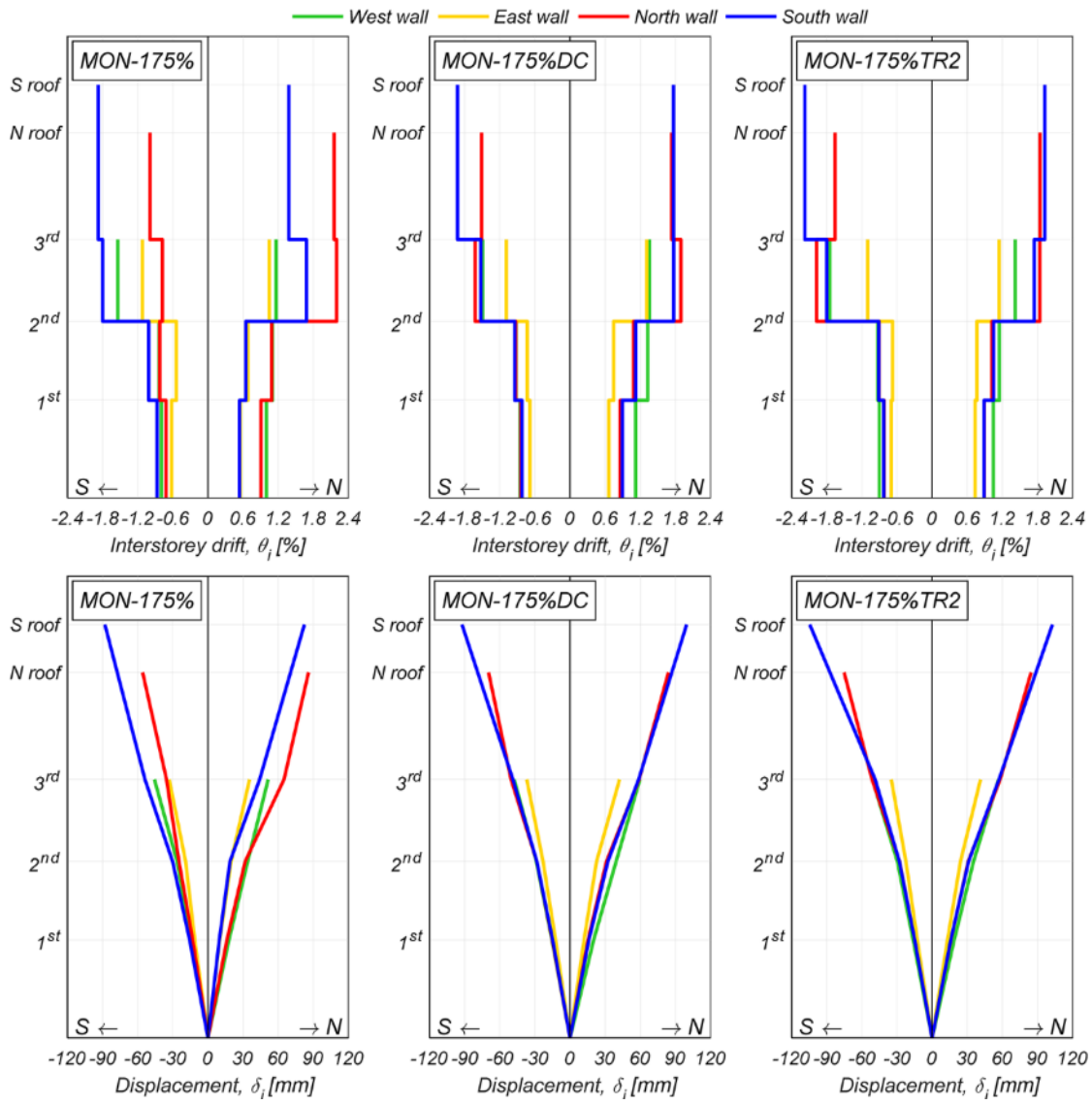

Figure 9. Interstorey drift-ratio and floor displacement envelopes. Tests with "MON" signal scaled at 175% before and after activation of the retrofit interventions.

552 Activation of the wall-to-diaphragm connections (test MON-175%DC, PGA of 0.34 g) and
553 tensioning of the tie rods (test MON-175%TR2, PGA of 0.37 g) had very similar effects
554 on the out-of-plane displacement and drift-ratio responses. The difference between the
555 envelopes of the North and South transverse walls became negligible, except for southward
556 gable overturning, proving the retrofit effectiveness at mitigating the separation observed
557 earlier. Residual out-of-plane rotations reduced from values ranging between 0.13% and
558 0.44% after test MON-175%, to negligible amounts, denoting a self-centring effect of
559 diaphragm connections and tie rods. No significant variations were instead appreciated on
560 the response of the longitudinal East and West façades.
561 Displacements and interstorey-drift ratios of the transverse walls did not exceed the
562 maximum measured on the longitudinal walls up to the second floor, indicating an overall
563 box-type behaviour of the first and second storeys of the prototype, without significant
564 local out-of-plane movements. For example, during test MON-175%DC the second-storey
565 out-of-plane rotations of the North and South walls in the negative direction (0.93%) were
566 nearly equal to the interstorey drift ratio of the West façade, while in the positive direction
567 (1.1%) were intermediate between the drift ratios recorded on the East and West façades
568 (0.75% and 1.3%, respectively). At the third storey, instead, the out-of-plane rotations of
569 the North and South walls (1.9% and 1.8%, respectively) remained larger than the
570 interstorey drift-ratios recorded on the East and West façades at the same level (1.3% and
571 1.4%, respectively), especially in the positive direction. In fact, the third-storey portion of
572 the transverse walls was still influenced by the gable out-of-plane overturning also with
573 fastened wall-to-diaphragm connections. Analogous trends were obtained from test MON-
574 175%TR2 after activation of the tie rods.

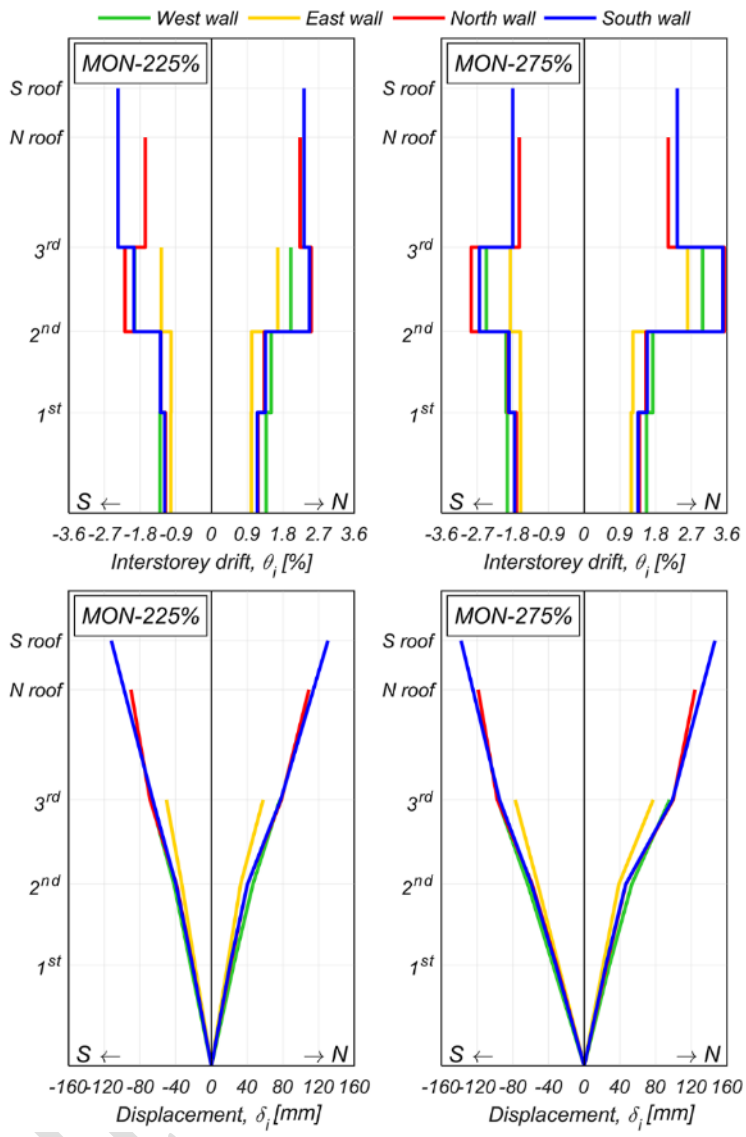

Figure 10. Interstorey drift-ratio and floor displacement envelopes. Tests with "MON" signal scaled at 225% and 275%, after activation of the retrofit interventions.

Similar observations can be extended to the behaviour of the prototype building aggregate during tests MON-225% (PGA of 0.51 g) and MON-275% (PGA of 0.64 g); despite reaching larger peak displacements (Figure 10), significant residual values did not develop through the end of the testing sequence. The envelopes recorded during the final test denoted a more pronounced concentration of out-of-plane rotation at the third storey, even though this effect was slightly visible also in previous test runs. The reasons for this

585 behaviour can be found in the stiffness offered to the gables by roof bracing, inducing a
586 softer third-story response, and in the development of a multiple-block rocking mechanism
587 over the height of the transverse façades. The latter mechanism is identifiable by horizontal
588 cracks at each floor level and along the gables, denoting the decomposition of the North
589 and South façades into several blocks which rocked out of their plane.

590 **4.5.Hysteretic response of the prototype**

591 Figure 11 and Figure 12 plot global hysteretic curves in terms of base shear (or base-shear
592 coefficient) versus third-floor average displacement (or average global drift ratio). Points
593 of maximum base-shear demand are highlighted by hollow dots, while points of maximum
594 displacement demand are marked with solid dots. Displacements and forces were defined
595 positive when directed northward. All residual displacements cumulated by the un-
596 retrofitted structure during main-shock and calibration tests were accounted for up to test
597 MON-175%. However, any previous residual displacement was disregarded for the tests
598 in strengthened configurations, as activation of wall-to-diaphragm connections and tie rods
599 resulted in almost complete recover of residual deformations.

600 Figure 11 depicts the hysteretic behaviour of the prototype during the tests under MON
601 signal scaled at 175%. In particular, the left-hand-side graph compares the response of the
602 un-retrofitted specimen during test MON-175% (PGA of 0.35 g) with the one during test
603 MON-100% (PGA of 0.20 g), when it experienced only minor structural damage:
604 significant stiffness degradation and energy dissipation can be observed. Peak global drift
605 ratio and base-shear coefficient of 0.92% and 0.35, respectively, were recorded in test
606 MON-175%. The central plot of Figure 11 shows that activation of the wall-to-diaphragm
607 connections allowed repeating the test (MON-175%DC, PGA of 0.34 g) with a stable

hysteretic response: maximum global drift ratio of 1.1% and base-shear coefficient of 0.36 were obtained, without appreciable stiffness degradation. Furthermore, tensioning the tie rods resulted in a similar response under two additional repetitions of the same input motion, up to test MON-175%TR2 (PGA of 0.37 g; right-hand-side graph), with a peak global drift ratio reduced to 1.0% and a base-shear coefficient increased to 0.39.

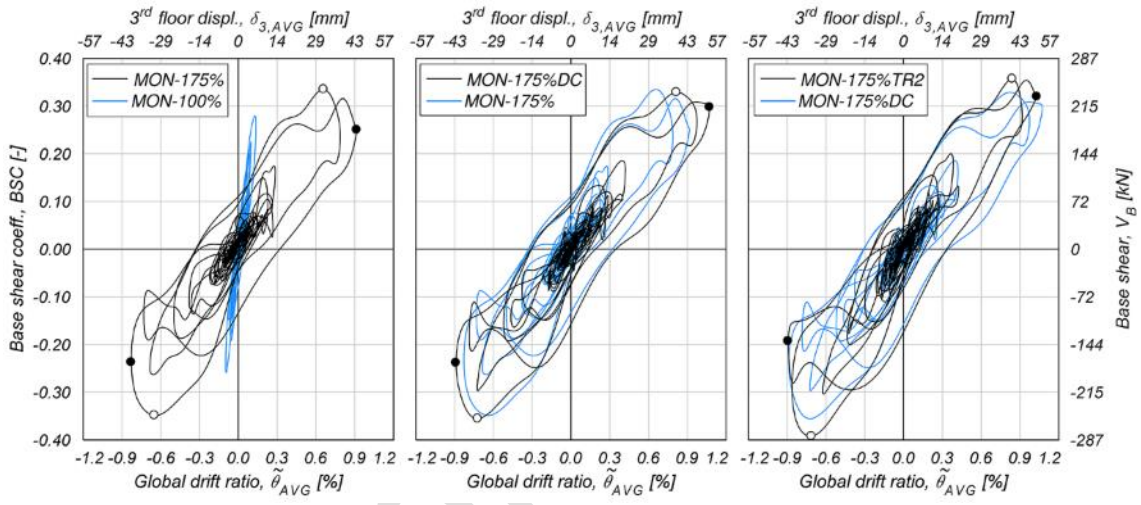

Figure 11. Global hysteretic response, accounting for residual displacements during the un-retrofitted testing phase. Tests with "MON" signal scaled at 175% before and after activation of the retrofit interventions.

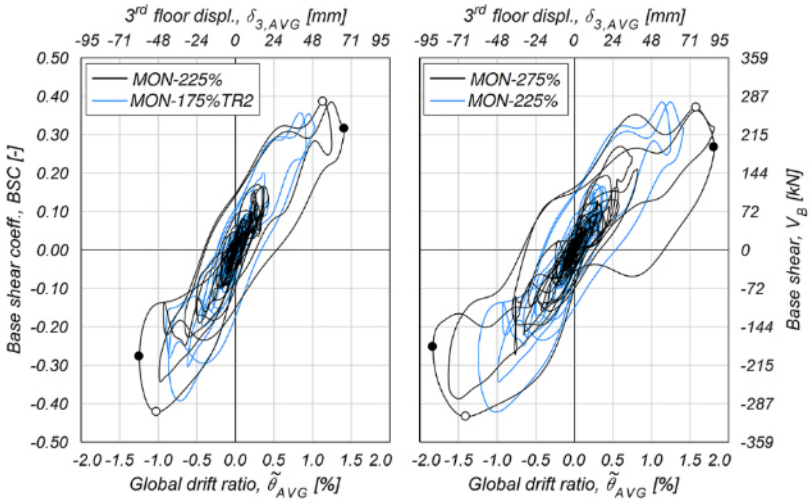

Figure 12. Global hysteretic response. Tests with "MON" signal scaled at 225% and 275%, after activation of the retrofit interventions.

When subjecting the retrofitted prototype to higher-intensity table motions (Figure 12), the prototype maintained its cracked stiffness and strength characteristics nearly unvaried, reaching peak drift ratios of 1.4% and of 1.8%, and base-shear coefficients of 0.42 and 0.43, during tests MON-225% (PGA of 0.51 g) and MON-275% (PGA of 0.64 g), respectively. Figure 13 shows the envelope of the prototype global hysteretic response in the positive (northward) direction, including all tests performed in the unstrengthened configuration. The backbone curve was built connecting the points with maximum base shear demand during each test, plus the point corresponding to the maximum displacement from test MON-275%. Cumulative residual displacements were accounted for as previously described. The envelope denotes a small strength enhancement due to retrofit activation and, more importantly, the ability of the strengthened structure to maintain its strength through the end of the testing sequence.

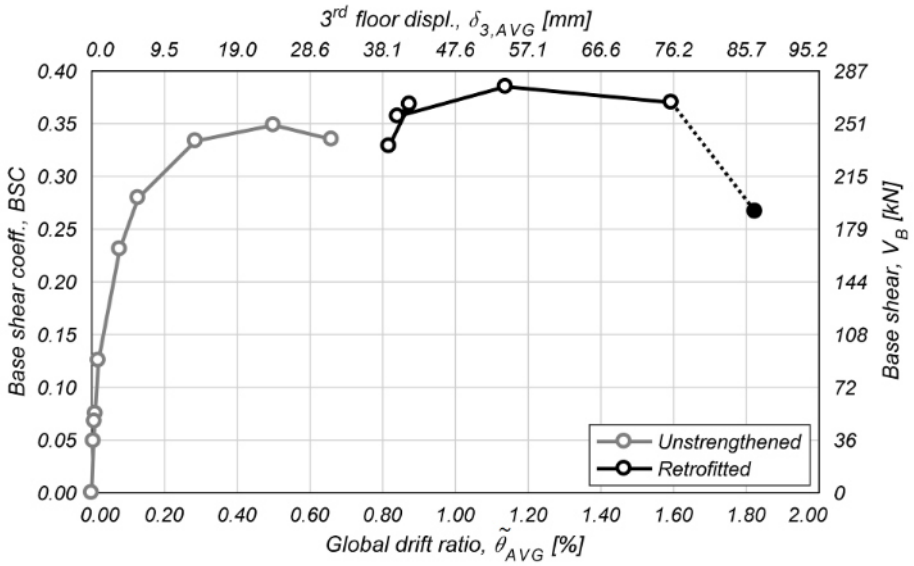

Figure 13. Envelope of the complete testing sequence, accounting for residual displacements during the un-retrofitted testing phase.

5. SUMMARY OF THE EXPERIMENTAL RESULTS

Figure 14 summarizes the prototype performance during the incremental shake-table test, in terms of peak and residual engineering demand parameters and fundamental period of vibration, for all tests including the un-retrofitted phase.

The peak average displacement ($\delta_{i,AVG}$) of the first three floors in the unstrengthened configuration were nearly proportional to the elevation up to test MON-125% (PGA of 0.26 g), with average interstorey drift ratios ($\theta_{i,AVG}$,) nearly equal. The two peak roof displacements ($\delta_{R,N}$ and $\delta_{R,S}$) were close to each other, and the corresponding roof-pitch shear deformations ($\gamma_{R,N}$ and $\gamma_{R,S}$) were about twice the lower interstorey drift ratios. As damage progressed, the maximum third-storey drift ratios approached the roof shear deformations in tests MON-150% and MON-175% (PGA of 0.32 g and 0.35 g). Activation of the retrofit systems allowed repeating the 175%-scaled MON input signal maintaining similar maximum displacement and deformation demands. The symmetry introduced by the retrofit between positive and negative displacement envelopes (Figure 9) corresponded to a reduction in the North (shorter) roof displacement and shear deformation demands. During all tests from MON-175%DC through MON-275% (PGA of 0.34 g through 0.64 g) the roof-pitch deformations remained nearly equal. In fact, since the masonry structure underneath the roof reached its lateral strength, it limited the acceleration transmitted to the base of the roof, even though the shake-table acceleration amplitude was increasing; because the roof was then excited by a nearly constant-amplitude input signal, its response did not vary significantly, as opposed to the table motion intensity.

Significant residual drift ratios were measured above the second-floor level from test MON-125%, reaching values of 0.19% to 0.26% at the end of test MON-175%. After activation of wall-to-diaphragm connections and tie rods, residual drift ratios were

dramatically reduced to less than 0.05% at all storeys. The proposed retrofit schemes effectively induced a self-centring behaviour on the building structure.

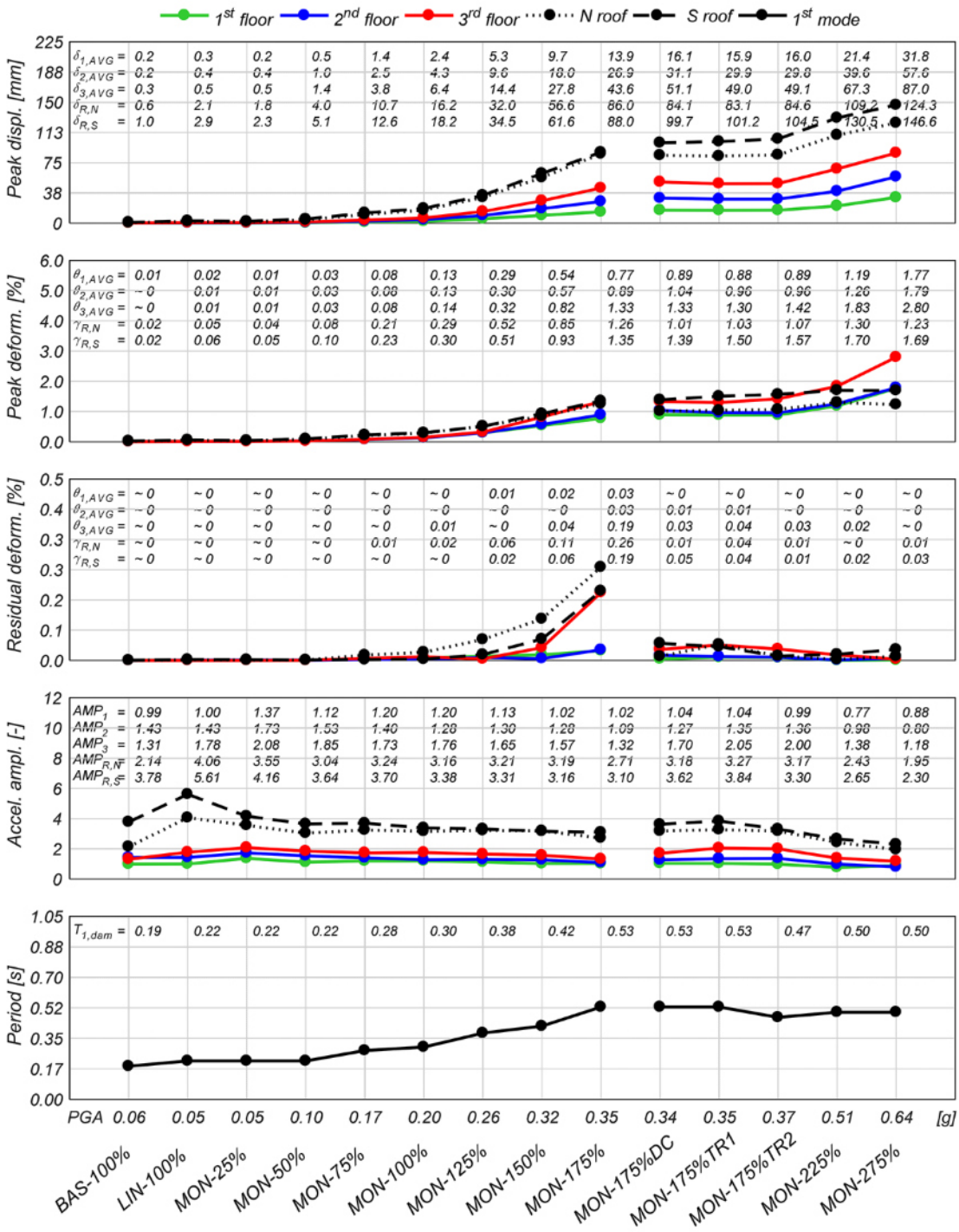

Figure 14. Summary of the prototype performance.

668 The acceleration amplification factor (AMP_i) was evaluated as the ratio between the i^{th}-
669 floor longitudinal average acceleration and the shake-table acceleration input. Figure 14
670 shows larger amplification at higher floors, as expected, with the roof factors reaching
671 almost twice the third-floor values. Considering the tests performed on the unstrengthened
672 specimen with MON signal, the acceleration amplification decreased for increasing PGA,
673 particularly from test MON-100% (PGA of 0.20 g) when about 80% of the lateral strength
674 was reached. In fact, the accelerations transmitted by the masonry walls to the supported
675 floors were limited by the walls lateral strength, once they entered the inelastic (ideally
676 plastic) range of response, while the shake-table acceleration amplitude was still
677 increasing. This in turn resulted in nearly constant output acceleration amplitudes of the
678 floors. After activation of the retrofit systems, which stabilized the building lateral strength,
679 the amplification factors remained nearly constant upon repetition of the 175%-scaled
680 MON signal. The decreasing trend reappeared as the input motion intensity was further
681 magnified, because the retrofit did not boost significantly the prototype strength and thus
682 the input acceleration transmitted to the floors, causing the floor accelerations to remain
683 almost unvaried as the shake-table motion intensity kept increasing.
684 The un-retrofitted building aggregate prototype exhibited a progressive fundamental-
685 period elongation, which was initially equal to 0.18 s, as damage propagated. The first
686 significant variation to 0.28 s was identified after the test MON-75%; after test MON-175%
687 it reached 0.53 s, almost three times the initial value. Activation of the retrofit interventions
688 allowed testing up to MON-275% without further fundamental-period elongation: at the
689 end of the sequence a value of 0.50 s was obtained, confirming the effectiveness of the

proposed retrofit interventions in delaying degradation of the dynamic properties of the structure.

6. CONCLUSIONS

This paper discussed the half-scale unidirectional shake-table test of a prototype stone masonry building aggregate, representative of heritage residential construction of the historical centre of Basel, Switzerland. The prototype was subjected to incremental dynamic tests, with input motions recorded during low-intensity seismic events in Switzerland or compatible with seismic scenarios for the city of Basel. The response of the unstrengthened masonry structure was compared with the enhanced behaviour obtained with retrofit solutions, consisting of (i) improved wall-to-diaphragm connections and (ii) steel tie rods.

The unstrengthened specimen exhibited minor structural damage after the test with PGA of 0.20 g and reached severe conditions during the test with PGA of 0.35 g. Significant damage occurred to the spandrels of the longitudinal East and West façades, with permanent elongation and separation between the two units at the roof base. Out-of-plane mechanisms were also activated during the test with PGA of 0.35 g, involving both North and South gables and the third-storey portion of the South façade. Longitudinal-façade piers underwent flexural-rocking response, but interlock between intersecting walls resulted in the participation of the southernmost third-storey piers in the overturning mechanism of the South façade. The asymmetrical distribution of first-storey openings caused differential displacement between the two longitudinal walls and in-plane shear deformation of the flexible floor diaphragms.

712 Prosecution of the shake-table testing campaign showed the effectiveness of the proposed
713 retrofit interventions. In particular, they allowed recovery of residual displacements and
714 deformations, and enhanced coupling of the out-of-plane responses of the transverse walls,
715 as demonstrated by similar displacement envelopes. Limiting separation between walls and
716 diaphragms, the two strengthening systems induced an overall box-type response of the
717 entire aggregate. Furthermore, the improved connection between gables and roof trusses
718 prevented local collapses due to out-of-plane overturning. The retrofit interventions
719 permitted repeating the input table motion with PGA of 0.35 g maintaining a stable
720 hysteretic response, with peak global drift ratio of approximately 1% and maximum base-
721 shear coefficient increasing from 0.35 in the unstrengthened configuration up to 0.39 after
722 post-tensioning the tie rods at 29 kN.
723 The strengthened prototype reached near-collapse conditions after testing at PGA of 0.64 g
724 when general de-cohesion of masonry was observed on the longitudinal walls, with fall of
725 small stones, portions of mortar, and debris. Separation between the two structural units
726 along the vertical joint extended for the full third-storey height. Multiple-block out-of-
727 plane rocking mechanisms developed on both transverse walls, while residual lintel
728 dislocations were observed on the North façade. Despite the severity of these conditions,
729 the retrofit interventions proved effective in minimizing residual displacements and
730 deformations, thus conferring to the structural system a self-centring behaviour, and in
731 preventing local collapses due to out-of-plane mechanisms. During the final test, the
732 specimen was subjected to a PGA of 0.64 g, which is 83% higher than the PGA imposed
733 before activating the retrofit devices. The retrofit systems allowed sustaining an ultimate
734 peak global drift ratio of 1.8%, which is almost twice the value of 0.92% recorded before

735 strengthening, and a base-shear coefficient of 0.43, that is 23% larger than the value of 0.35
736 resisted before retrofit activation.
737 The results of this experimental study, in both unstrengthened and retrofitted configuration,
738 constitute a useful benchmark to calibrate numerical models, which can be extended to full
739 scale situations and different retrofit solutions. Valuable information is provided for the
740 development of sophisticated numerical models or for the implementation of the out-of-
741 plane response in simpler equivalent-frame models, to capture the combined longitudinal
742 and transverse response of masonry aggregates. Moreover, the results from the numerical
743 simulations of the prototype response can form the basis of vulnerability studies on more
744 complex building aggregates, considering the interaction between several structural units,
745 with different interstorey height or diaphragm stiffnesses, and including the effect of
746 localized retrofit interventions.
747

748 **ACKNOWLEDGEMENTS**

749 The work presented is part of the research project “Seismic assessment of natural stone
750 masonry buildings in Basel - A research and training project”, jointly carried by the École
751 Polytechnique Fédérale de Lausanne and the University of Pavia, which was supported by
752 the Swiss Federal Office for the Environment and the Construction Department of the
753 Canton Basel-Stadt.
754 The authors would like to thank Mapei S.p.a. for its support to the project. The help
755 provided during the tests by M. Caruso, P. Comini, F. Dacarro, F. Di Santo, S. Girello, L.
756 Grottoli, M. Mandirola, B. Marchesi and U. Tomassetti is gratefully acknowledged.

Any opinions, finding and conclusions expressed in this paper are those of the authors and do not necessarily reflect the views of the sponsors.

REFERENCES

Arias A (1970) A measure of earthquake intensity. In: Hansen RJ, editor. Seismic Design of Nuclear Power Plants. MIT Press, Cambridge, Massachusetts, United States, p. 438-483.

Benedetti D, Carydis P, Pezzoli P (1998) Shaking table test on 24 masonry buildings. Earthquake Engineering & Structural Dynamics, 27(1), 67-90.

Bianchini M, Diotallevi P, Baker JW (2009) Prediction of inelastic structural response using an average of spectral accelerations. In: Proc. 10th International Conference on Structural Safety and Reliability, Osaka, Japan.

Bradley BA (2011) Correlation of significant duration with amplitude and cumulative intensity measures and its use in ground motion selection. Journal of Earthquake Engineering, 15(6), 809-832.

Calderini C, Lagomarsino S, Rossi M, De Canio G, Mongelli ML, Roselli I (2015) Shaking table tests of an arch-pillars system and design of strengthening by the use of tie-rods. Bulletin of Earthquake Engineering, 13(1), 279-297.

Calderini C, Piccardo P, Vecchiattini R (2019) Experimental characterization of ancient metal tie-rods in historic masonry buildings. International Journal of Architectural Heritage, 13(3), 425-437.

Carocci CF (2012) Small centres damaged by 2009 L'Aquila earthquake: on site analyses of historical masonry aggregates. Bulletin of Earthquake Engineering, 10(1), 45-71.

780 Celik O, Sesigur H, Cili F (2009) Importance of wood and iron tension members on seismic
781 performance of historic masonry buildings: Three case studies from Turkey. In: Proc
782 ATC and SEI Conference on Improving the Seismic Performance of Existing Buildings
783 and Other Structures, San Francisco, California, United States.
784 da Porto F, Munari M, Prota A, Modena C (2013) Analysis and repair of clustered
785 buildings: Case study of a block in the historic city centre of L'Aquila (Central Italy).
786 Construction and Building Materials, 38, 1221-1237.
787 Fäh D, Huggenberger P (2006) Erdbebenmikrozonierung am Südlichen Oberrhein.
788 Zusammenfassung für das Projektgebiet Gebiet in der Schweiz. Report. Available from
789 the authors upon request (in German).
790 Fäh D, Gisler M, Jaggi B, Kästli P, Lutz T, Masciadri V, Matt C, Mayer-Rosa D, Rippmann
791 D, Schwartz-Zanetti G, Tauber J, Wenk T (2009) The 1356 Basel earthquake: an
792 interdisciplinary revision. Geophysical Journal International, 178(1), 351-374.
793 Fäh D, Wenk T (2009) Mikrozonierung für die Kantone Basel Stadt und Basel Landschaft,
794 Optimierung der Form der Antwortspektren und der Anzahl der Mikrozonen. Report,
795 Swiss Seismological Service, ETH, Zurich, Switzerland (in German).
796 Formisano A (2017) Theoretical and numerical seismic analysis of masonry building
797 aggregates: case studies in San Pio Delle Camere (L'Aquila, Italy). Journal of
798 Earthquake Engineering, 21(2), 227-245.
799 Formisano A, Florio G, Landolfo R, Mazzolani FM (2015). Numerical calibration of an
800 easy method for seismic behaviour assessment on large scale of masonry building
801 aggregates. Advances in Engineering Software, 80, 116-138.

802 Graziotti F, Penna A, Magenes G (2016) A nonlinear SDOF model for the simplified
803 evaluation of the displacement demand of low-rise URM buildings. Bulletin of
804 Earthquake Engineering, 14(6), 1589-612.
805 Grünthal G, editor. (1998) European Macroseismic Scale 1998 (EMS-98). Cahiers du
806 Centre Européen de Géodynamique et de Séismologie 15. Centre Européen de
807 Géodynamique et de Séismologie, Luxembourg.
808 Guerrini G, Senaldi I, Scherini S, Morganti S, Magenes G, Beyer K, Penna A (2017)
809 Material characterization for the shaking-table test of the scaled prototype of a stone
810 masonry building aggregate. In: Proc. 17th ANIDIS Conference, Pistoia, Italy.
811 Hancock J, Bommer JJ (2006) A state-of-knowledge review of the influence of strong-
812 motion duration on structural damage. Earthquake Spectra, 22(3), 827-845.
813 Magenes G, Penna A, Galasco A (2010) A full-scale shaking table test on a two-storey stone
814 masonry building. In: Proc. 14th European Conference on Earthquake Engineering,
815 Ohrid, Republic of Macedonia.
816 Magenes G, Penna A, Senaldi IE, Rota M, Galasco A (2014) Shaking table test of a
817 strengthened full-scale stone masonry building with flexible diaphragms. International
818 Journal of Architectural Heritage, 8(3), 349-375.
819 Maio R, Vicente R, Formisano A, Varum H (2015). Seismic vulnerability of building
820 aggregates through hybrid and indirect assessment techniques. Bulletin of Earthquake
821 Engineering, 13(10), 2995-3014.
822 Mazzon N, Chavez CM, Valluzzi MR, Casarin F, Modena C (2010) Shaking table tests on
823 multi-leaf stone masonry structures: Analysis of stiffness decay. Advanced Materials
824 Research, 133, 647-652.

825 Modena C, Valluzzi MR, Garbin E, da Porto F (2005) A strengthening technique for timber
826 floors using traditional materials In: Proc. 4th Structural Analysis of Historical
827 Constructions Conference, Padova, Italy.
828 Moreira S, Ramos LF, Oliveira DV, Lourenço PB (2014) Experimental behavior of
829 masonry wall-to-timber elements connections strengthened with injection anchors.
830 Engineering Structures, 81, 98-109.
831 Moreira S, Ramos LF, Oliveira DV, Lourenço PB (2016) Design parameters for
832 seismically retrofitted masonry-to-timber connections: injection anchors. International
833 Journal of Architectural Heritage, 10(2-3), 217-234.
834 Mouzakis C, Adami CE, Karapitta L, Vintzileou E (2018). Seismic behaviour of timber-
835 laced stone masonry buildings before and after interventions: shaking table tests on a
836 two-storey masonry model. Bulletin of Earthquake Engineering, 16(2), 803-829.
837 Podestà S, Scandolo L (2019) Earthquakes and Tie-Rods: Assessment, Design, and
838 Ductility Issues. International Journal Of Architectural Heritage, 13(3), 329–339
839 Ripperger J, Kästli P, Fäh D, Giardini D (2009). Ground motion and macroseismic
840 intensities of a seismic event related to geothermal reservoir stimulation below the city
841 of Basel - observations and modelling. Geophysical Journal International, 179(3), 1757-
842 1771.
843 Senaldi I, Magenes G, Penna A (2010) Numerical investigations on the seismic response
844 of masonry building aggregates. Advanced Materials Research, 133, 715-720.
845 Senaldi I, Magenes G, Penna A, Galasco A, Rota M (2014) The effect of stiffened floor
846 and roof diaphragms on the experimental seismic response of a full-scale unreinforced
847 stone masonry building. Journal of Earthquake Engineering, 18(3), 407-443.

Senaldi I, Guerrini G, Comini P, Graziotti F, Magenes G, Beyer K, Penna A (2019) Experimental seismic response of a half-scale stone masonry building aggregate. Bulletin of Earthquake Engineering, https://doi.org/10.1007/s10518-019-00631-2

SIA 261:2014 (2014) Einwirkungen auf Tragwerke. Swiss Society of Engineers and Architects, Zurich, Switzerland (in German).

Swiss Seismological Service, "SED Strong-Motion Portal," 2017. Available: strongmotionportal.seismo.ethz.ch. [Accessed: 21-Mar-2017].

Tomaževič M, Lutman M, Weiss P (1996) Seismic upgrading of old brick-masonry Urban Houses: Tying of walls with steel ties. Earthquake Spectra 12 (3):599–622.

Tomaževič M, Weiss P, Velechovsky T (1991) The influence of rigidity of floors on the seismic behaviour of old stone-masonry buildings, European Earthquake Engineering, 3, 28-41.

Valluzzi MR (2007) On the vulnerability of historical masonry structures: analysis and mitigation. Materials and Structures, 40(7), 723-743.

Vicon Motion Systems (2016) Vicon Nexus user guide. Centennial, Colorado, United States. Available at URL: https://www.vicon.com. [Accessed: 18-Jun-2019]

Vintzileou E, Mouzakis C, Adami CE, Karapitta L (2015) Seismic behavior of three-leaf stone masonry buildings before and after interventions: Shaking table tests on a two-storey masonry model. Bulletin of Earthquake Engineering, 13(10), 3107-3133.

Wenk T, Fäh D (2012) Seismic Microzonation of the Basel Area. In: Proc. 15th World Conference on Earthquake Engineering, Lisbon, Portugal.

869 Wiemer S, Danciu L, Edwards B, Marti M, Fäh D, Hiemer S, Wössner J, Cauzzi C, Kästli
870 P, Kremer K (2016) Seismic Hazard Model 2015 for Switzerland (SUIhaz2015). Report,
871 Swiss Seismological Service, ETH, Zurich, Switzerland.
872